

## Highlights

### **FE-MCFormer: An interpretable fault diagnosis framework for rotating machinery under strong noise based on time-frequency fusion transformer**

Yuhan Yuan, Xiaomo Jiang, Haibin Yang, Haixin Zhao, Shengbo Wang, Xueyu Cheng, Jigang Meng, Shuhua Yang

- Proposed a novel interpretable fault diagnosis method for rotating machinery under strong noise.
- Developed a Fourier adaptive reconstruction embedding layer to enhance model performance.
- Designed a time-frequency fusion module to extract multi-dimensional features.
- Validated the methodology through two laboratory test datasets and one real-world industrial dataset.

# FE-MCFormer: An interpretable fault diagnosis framework for rotating machinery under strong noise based on time-frequency fusion transformer

Yuhan Yuan<sup>a</sup>, Xiaomo Jiang<sup>a,b,c,\*</sup>, Haibin Yang<sup>a</sup>, Haixin Zhao<sup>a</sup>, Shengbo Wang<sup>a</sup>, Xueyu Cheng<sup>d</sup>, Jigang Meng<sup>a</sup> and Shuhua Yang<sup>e</sup>

<sup>a</sup>School of Energy and Power Engineering, Dalian University of Technology, Dalian, 116024, China

<sup>b</sup>State Key Lab of Structural Analysis, Optimization and CAE Software for Industrial Equipment, Dalian University of Technology, Dalian, 116024, China

<sup>c</sup>Provincial Key Lab of Digital Twin for Industrial Equipment, Dalian University of Technology, Dalian, 116024, China

<sup>d</sup>College of Arts and Sciences, Clayton State University, Morrow, GA, 30260, USA

<sup>e</sup>Shenyang Blower Works Group Corporation, Liaoning, 110869, China

## ARTICLE INFO

### Keywords:

Rotating machinery  
Fault diagnosis  
Transformer model  
Interpretable  
Frequency domain reconstruction

## ABSTRACT

Many fault diagnosis methods of rotating machines are based on discriminative features extracted from signals collected from the key components such as bearings. However, under complex operating conditions, periodic impulsive characteristics in the signal related to weak fault information are often obscured by noise interference. Consequently, existing approaches struggle to learn interpretable fault-related features in such scenarios. This paper proposes a novel transformer framework (FE-MCFormer) to extract interpretable time-frequency features, with the aim of improving the fault detection accuracy and interpretability of rotating machines under strong noise. First, a Fourier adaptive reconstruction embedding layer is introduced as a global information encoder in the model. Subsequently, a time-frequency fusion module is designed, further improve the model robustness and interpretability. The effectiveness of FE-MCFormer in machine fault diagnosis is validated through three case studies.

## 1. Introduction

As an irreplaceable part of modern industrial system, rotating machinery plays a vital role in industrial manufacturing [1, 2]. The health status of rotating parts, such as bearings, directly affects the reliability and safety of the entire mechanical system. The failure of rotating parts during operation often causes catastrophic failures and huge economic losses [3]. Therefore, it is of paramount importance to carry out effective condition monitoring and fault diagnosis for rotating machines.

In general, existing fault diagnosis (FD) methods for rotating machinery are categorized into three main types: traditional, machine learning, and deep learning. Traditional methods are mainly rely on features extracted from time, frequency, or time–frequency domains of signals through various transform techniques, such as Fourier Transform (FT), wavelet transform (WT), empirical mode decomposition (EMD), empirical wavelet transform (EWT), and variational mode decomposition (VMD). Jiang et al. [4] proposed a time–frequency modulation approach of the spectral amplitude to capture the characteristic frequencies of vibration

signals. Xu et al. [5] introduced a DS-based adaptive spectrum reconstruction method for the recognition of rolling bearings state. Chen et al. [6] developed a hierarchical improved envelope spectrum entropy method to extract intrinsic fault features of mechanical vibration signals. Kou et al. [7] applied an improved complete ensemble EMD with empirical entropy (EE) to extract features and validated the method on mine hoist sheave bearing fault detection. Zhou et al. [8] proposed a continuous hierarchical fractional range entropy approach for machine FD in noisy environments. Clearly traditional methods have significantly advanced the development of FD. However, they rely heavily on expert knowledge and data quality, making them resource intensive and inaccurate under incomplete data.

Compared with traditional approaches, machine learning (ML) methods can extract more valuable fault characteristics from large historical datasets, making them a promising approach for machinery FD. For example, Ren et al. [9] introduced an unsupervised across-tasks meta-learning strategy to enable few-shot FD under varying working conditions. Chen et al. [10] developed a meta-learning approach for bearing fault detection and classification under varying working conditions with limited data. Zhang et al. [11] proposed a representation-based transfer learning method to enhance few-shot bearing fault classification. However, machine learning approaches exhibit limitations in modeling high-dimensional, highly accurate, and nonlinear variations, which can hinder their effectiveness in complex industrial scenarios.

\*Corresponding author at: State Key Lab of Structural Analysis, Optimization and CAE Software for Industrial Equipment, Dalian University of Technology, Dalian, 116024, China.

 yuhanyuan@mail.dlut.edu.cn (Y. Yuan);

xiaomojiang2019@dlut.edu.cn (X. Jiang); yanghaibin@mail.dlut.edu.cn (H. Yang);

zhaohaixin@dlut.edu.cn (H. Zhao); s2013566862@mail.dlut.edu.cn (S. Wang);

xueyucheng@clayton.edu (X. Cheng);

mengjigang@mail.dlut.edu.cn (J. Meng); yshemail@sina.com (S. Yang)

In recent decade, various deep learning (DL) methods have been widely used to improve the safety and reliability of industrial equipment. Compared with ML methods, DL approaches require less manual feature engineering, while having obvious advantages on processing massive measured data. For example, the multiscale convolutional neural network (MSCNN), as one of the popular deep learning models, has been widely used in signal processing. Shao et al. [12] proposed a novel multiscale network for few-shot bearing fault diagnosis. Wang et al. [13] proposed a multiscale deep attention Q network for gearbox fault diagnosis. Xu et al. [14] presented a multiscale dense CNN model combined with a modified hierarchical procedure for the identification of rolling bearing failure. Jia et al. [15] proposed a multiscale residual attention convolutional network to extract multiscale features and reduce noise from vibrational signals. Han et al. [16] proposed a lightweight multiscale attention deep network (MSADN) for interpretable in-situ remaining useful life (RUL) prediction of industrial robots. These methods have promoted the application of multiscale CNN in the diagnosis of rotating machine faults.

However, the aforementioned studies failed to take into account strong noise interference in the diagnosis of rotating machinery faults. Although CNNs are capable of extracting local features and identifying periodic patterns in signals, the harsh environment and varying operation scenarios introduce strong interference and uncertainty into the sensor data. As a result, acquired signals often contain noise components to some degree, making fault features overwhelmed by noise components. This results in the difficulty of fault diagnosis of rotating machinery using CNN methods.

As another powerful DL method, the transformer, is helpful to address the aforementioned limitations. Transformer-based model has been successfully applied for fault diagnosis of rotating machinery. For example, Li et al. [17] proposed an interpretable variational transformer with Dirichlet prior for fault diagnosis. Ding et al. [18] came up with the novel time-frequency transformer to achieve fault diagnosis and demonstrated its superiority. Zhang et al. [19] proposed an interpretable rotating machinery fault diagnosis framework based on KAN-Transformer (KANTF). Han et al. [20] proposed the Convformer-NSE, which utilizing sparse modified multi head self-attention to achieve robust fault diagnosis of gearboxes through the integration of global and local information. However, the characteristic of multi-head self attention (MHSA) lead to the grow of computing cost quadratically with the increase of input sequence length, which is costly for fault diagnosis of rotating machines with 1000 or more samples for a single variable. In addition, due to the lack of inherent local modeling capability in MHSA, transformer method may under-perform compared to MSCNN in scenarios where local feature extraction is critical.

According to the aforementioned literature review, deep learning models for rotating machinery fault diagnosis still suffer from two major limitations.

- 1) Although MSCNNs have demonstrated strong performance across various domains [16, 21, 22], their effectiveness in noisy environments remains limited due to the inherent characteristics of convolution. Additionally, there is still a lack of research of interpretable MSCNN model under strong noisy environment.
- 2) While transformers have demonstrated remarkable capabilities in long-range dependencies, the MHSA mechanism often becomes a performance bottleneck in certain scenarios due to its high computational complexity and weak local bias. Current approaches transformers focus on improving the local feature extraction of MHSA [23, 20, 24]. However, recent studies [25, 26] have revealed that other components of the transformer, including the feed-forward network (FFN), residual connections, and normalization layers, also play crucial roles in overall performance. Notably, even transformer variants that discard MHSA altogether have shown superior performance in specific applications [27, 28].

Therefore, in order to effectively combine the strengths of MSCNN and transformer to achieve interpretable fault diagnosis under strong noise interference, this study proposes a novel transformer-inspired framework named FE-MCFormer, thus improving the diagnostic performance with noise disturbance and interpretability. In FE-MCFormer, a Fourier adaptive reconstruction embedding layer (FAREL) is proposed for global encoding and frequency-domain adaptive reconstruction. In addition, an efficient and interpretable multiscale convolutional attention layer (MSCAL) is designed to replace the conventional MHSA in transformers. Furthermore, a time-frequency fusion network (TFFN) is developed to enhance the model's robustness and nonlinear ability. The major contributions of this study are summarized as follows:

- 1) A novel transformer-based framework, named FE-MCFormer, is designed that combines the strengths of MSCNN and the transformer architecture. FE-MCFormer models both local time-domain features and global frequency-domain information. This allows it to extract rich time-frequency fusion features, which are particularly suitable for fault diagnosis of rotating machines under strong noise conditions.
- 2) A Fourier adaptive reconstruction embedding layer (FAREL) is proposed to enhance the noise robustness and interpretability of the model. Experimental results show that FAREL not only enhances the model robustness and interpretability, but also shows great potential as a plug-and-play component for performance improvement in FD task.
- 3) To further extract time-frequency fusion features and improve the model's noise robustness and nonlinearity, a multiscale time-frequency fusion (MSTFF) module is introduced. The MSTFF module consists of (a) an interpretable multiscale convolutional attention layer (MSCAL) for extracting local multiscale time-domain features, and (b) a time-frequency fusion network (TFFN) to enhance the ability of global and nonlinear modeling.

- 4) Case studies on two test bench datasets and a real-world industrial dataset are conducted to verify the effectiveness and practicality of the proposed FE-MCFormer model for FD of rotating machines. Sensitivity analysis and ablation studies are also performed to validate the necessity of each component in FE-MCFormer.

The remainder of this study is organized as follows. Section 2 presents the proposed FE-MCFormer in detail. In Section 3, three case studies are conducted to verify the effectiveness and interpretability of FE-MCFormer in the FD task of the rotating machine. Finally, Section 4 concludes this study.

## 2. Methodology

Fig. 1 shows the architecture of the proposed method, which is mainly composed of a Fourier adaptive reconstruction embedding layer (FAREL), several Multiscale Time-Frequency Domain Fusion (MSTFF) modules, which contain a Multiscale Convolution Attention Layer (MSCAL) and a Feedforward Layer (FFL) with two batch normalization layers, three distillation layers, and a fault classification layer. Specifically, the signal is first input into the FAREL for frequency-domain reconstruction and global feature learning. Then, the distillation layer is utilized to prioritize the superior key features. Furthermore, several MSTFF modules and distillation layers are leveraged to further extract time-frequency features. Finally, the extracted features are subsequently input into a fully connected layer and a softmax layer to obtain the reliability status of the monitored machinery.

### 2.1. Fourier adaptive reconstruction embedding layer (FAREL)

The FAREL is introduced as the embedding layer. Given the input time-series signal  $x \in \mathbb{R}^{B \times 1 \times L}$ , a  $1 \times 63$  convolutional operation is applied to transform the  $x$  to a higher dimension, represented by  $(x_1, \dots, x_c) \in \mathbb{R}^{B \times C \times L}$ , where  $c$  denotes the number of channels. Then, a discrete Fourier Transform (DFT) is utilized to convert the time-domain feature to the frequency-domain:

$$F[(x_1, \dots, x_n)] = (a_1 + ib_1, \dots, a_n + ib_n) = A + iB \quad (1)$$

where  $F[\cdot]$  denotes the DFT operation, and  $A + iB$  represents the resulting complex spectrum composed of real and imaginary parts. Physically, this operation corresponds to decomposing the signal into orthogonal frequency components, enabling the network to highlight fault-related spectral features that may be buried under broadband noise. We then apply a learnable complex spectrum weight  $W$  to adaptively reconstruct the frequency components as follows:

$$W = (w_1^r + iw_1^m, \dots, w_n^r + iw_n^m) \quad (2)$$

where  $w_i^r$  and  $w_i^m$  represents the real and imaginary parts of the learnable weight  $W$ , respectively. All elements of  $W$  are updated through back-propagation. Then, we perform

element-wise multiplication (also known as Hadamard product) between the transformed data  $A + iB$  and the learnable weight  $W$ , yielding the adaptively filtered frequency-domain representation:

$$\begin{aligned} A' + iB' \\ = (a_1 + ib_1, \dots, a_n + ib_n) \otimes (w_1^r + iw_1^m, \dots, w_n^r + iw_n^m) \end{aligned} \quad (3)$$

where  $\otimes$  denotes the Hadamard product,  $A'$  and  $B'$  represent the reconstructed real and imaginary components. After adaptive frequency-domain adjustment, an inverse DFT is applied to recover the modified signal back into the time-domain:

$$(x_1', \dots, x_n') = F^{-1} [(A' + iB')] \quad (4)$$

where  $F^{-1}[\cdot]$  represents the inverse Fourier Transform. Further, the reconstructed signal is then subjected to an element-wise addition operation with original feature map  $(x_1, \dots, x_n)$  as the reconstructed signal, i.e.,

$$(x_1^r, \dots, x_n^r) = (x_1, \dots, x_n) + \gamma \cdot (x_1', \dots, x_n') \quad (5)$$

where  $x_i^r$  stands for the reconstructed signal,  $\gamma$  denotes the scaling factor. various tasks and data properties. Finally, the entire FAREL can be expressed as:

$$\begin{aligned} FAREL(x) \\ = conv(x) + \gamma \cdot F^{-1} \{W \otimes F[conv(x)]\} \end{aligned} \quad (6)$$

where  $x$  denotes the input signal,  $conv(\cdot)$  stands for the convolutional operation, FAREL serves as a global encoder, effectively integrating local patterns with frequency-domain global dependencies in an adaptive and differentiable manner.

### 2.2. MSTFF module

MSTFF is designed to extract multiscale time-frequency fusion features and suppress irrelevant information. It comprises a multiscale convolutional attention layer (MSCAL) and a time-frequency fusion network (TFFN). As shown in Fig. 1, a MSTFF consists of a multiscale convolution attention layer (MSCAL) and a time-frequency fusion network (TFFN) with two batch-norm layers.

#### 2.2.1. Multiscale convolution attention layer

MSCAL is proposed to extract multiscale time-domain features with high efficiency and interpretability. As shown in Fig. 1, first, given the input  $x$ , a  $1 \times 1$  convolution kernel is utilized as the channel communication kernel, i.e.,

$$y_1 = conv_{1 \times 1}(x) \quad (7)$$

Then, two parallel branches with  $1 \times 3$  and  $1 \times 5$  convolutional operations are introduced to extract multiscale time-domain features as follows:

$$y_2 = \sum_{i=1}^2 Branch_i[y_1] \quad (8)$$

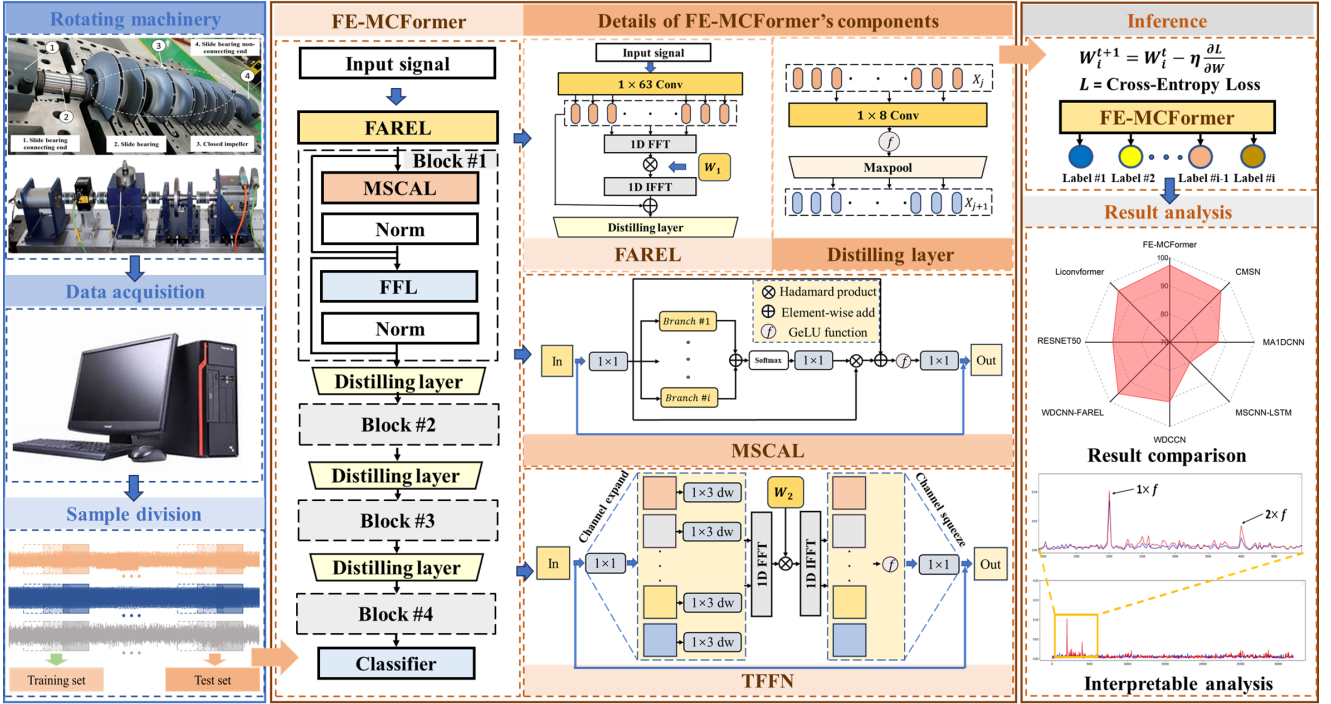


Fig. 1. Diagnosis framework for the rotary machine with FE-MCFormer.

where  $Branch_i[\cdot]$  denotes the two feature branches with  $1 \times 3$  and  $1 \times 5$  convolutional operations, which are sensitive to local fault features. Further, a softmax function is applied to scale multiscale features in the range of  $[0, 1]$ , and another  $1 \times 1$  convolution kernel is utilized to fuse the multiscale information. The Hadamard product is performed between fusion features and feature map  $y_1$ , and the residual connection is linked between  $y_1$  and the output features, given as follows:

$$y_3 = \begin{cases} conv_{1 \times 1}(attn) \otimes y_1 + y_1 \\ attn = softmax(y_2) \end{cases} \quad (9)$$

where  $\otimes$  denotes the Hadamard product, and  $softmax(\cdot)$  stands for the softmax function. Finally, a Gaussian error linear unit (GELU) function is employed as the activation layer, and a  $1 \times 1$  convolution kernel is introduced as another channel communication kernel. Ultimately, the residual structure is employed to prevent gradient vanishing or explosion, given by:

$$y_4 = conv_{1 \times 1}[GELU(y_3)] + x \quad (10)$$

### 2.2.2. Time-frequency fusion network

Traditional feedforward networks (FFN) have limited capability in modeling global contextual information, thus losing global dependency after multiple iterations. To extract global information and further filter out irrelevant information in frequency-domain, we introduce the time-frequency fusion network (TFFN), in TFFN, a Fourier adaptive reconstruction (FAR) operation, which is similar to FAREL, is introduced to reconstruct the input tensor in frequency-domain. As shown in Fig. 1, given the input feature  $X \in$

$\mathbb{R}^{C \times L}$ , the TFFN first applies a  $1 \times 1$  convolutional operation to increase the dimensionality of feature representation, given by:

$$\bar{X} \in \mathbb{R}^{2C \times L} = conv_{1 \times 1}^{ex}(X \in \mathbb{R}^{C \times L}) \quad (11)$$

where  $conv_{1 \times 1}^{ex}(\cdot)$  represents the  $1 \times 1$  convolutional with channel expand operation. Then, a  $1 \times 3$  depthwise convolutional operation is employed to extract local features, followed by a GELU activation to enhance nonlinear representational capacity, as follows:

$$\dot{X} = GELU[conv_{1 \times 3}^{dw}(\bar{X})] \quad (12)$$

where  $GELU$  denotes the activation function, and  $conv_{1 \times 3}^{dw}(\cdot)$  represents the  $1 \times 3$  depthwise convolutional operation. Further, a DFT is utilized to transform the time-domain feature into the frequency-domain ones, that is

$$X' = F[\dot{X}] \quad (13)$$

where  $F[\cdot]$  denotes the DFT operation. Then, a learnable weight  $W$  is introduced to reconstruct the feature in frequency-domain, and a scaling factor is utilized to maintain the numerical stability, defined by:

$$\hat{X} = X' \otimes W \cdot \gamma \quad (14)$$

where  $\hat{X}$  represents the reconstruction feature,  $\otimes$  stands for the Hadamard product, and  $\gamma$  denotes the scaling factor. Moreover, an inverse DFT is performed on the reconstruction feature back into the time-domain, where the reconstruct

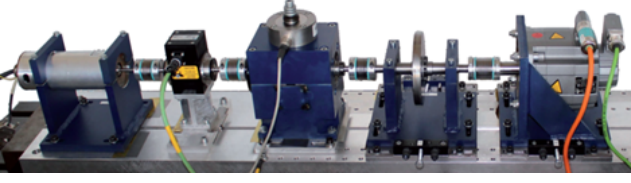


Fig. 2. Rolling bearing test rig. (Case 1)

feature uses a  $1 \times 1$  convolutional operation to transform it back into the time-domain, given by:

$$\check{X} \in R^{C \times L} = conv_{1 \times 1}^{se}[F^{-1}(\hat{X})] \quad (15)$$

where  $conv_{1 \times 1}^{se}(\cdot)$  denotes the  $1 \times 1$  convolutional operation with channel squeeze, and  $F^{-1}[\cdot]$  stands for the inverse DFT. Finally, the reconstructed features are added element-wise to the original feature  $X$  as the final output of TFFN:

$$X^r = X + \check{X} \quad (16)$$

where  $X^r$  denotes the output features of TFFN.

### 2.2.3. Distillation layer

The distilling operation is designed to privilege the superior ones with time-dominant features and create a focused global feature map in the next MSTFF module. It trims the input's time dimension sharply, with distilling procedure forwarding from the  $j$ -th layer to the  $(j+1)$ -th layer, defined as follows:

$$\begin{aligned} X_{j+1}^{2C \times \frac{L}{2}} \\ = \text{MaxPool} \left( \text{GELU} \left( \text{Conv1d} \left( \left[ X_j^{C \times L} \right]_{MS} \right) \right) \right) \end{aligned} \quad (17)$$

where  $[\cdot]_{MS}$  represents the MSTFF module, and  $\text{Conv1d}$  performs a 1-D convolutional operation on the time-domain with the GELU activation function.  $C$  and  $L$  denote the channel numbers and length of  $X$ , respectively. We expand the number of channels by using a  $1 \times 5$  convolutional operation and employ a max-pooling layer with the kernel size of 3 and the stride size of 2 to downsample  $X$  into its half-slice after stacking a layer, which reduces the overall memory usage of next MSTFF module.

## 3. Experimental Verification

In this section, three case studies are conducted to verify the adaptability and practicability of FE-MCFormer and FAREL in the fault detection of rotating machines. The laboratory test datasets are employed in Case 1 and Case 2 while the actual measurements from a real-world centrifugal compressor are utilized in Case 3.

### 3.1. Experimental settings

The FE-MCFormer code is compiled in the PyTorch framework on a workstation with an Intel(R) Xeon(R) Gold

Table 1  
Structural parameters of FE-MCFormer.

Component	Layer name	Parameters	Output size
	Input	/	$1 \times 2048$
Embedding layer	FAREL	kernel size = 63, stride = 1	$32 \times 2048$
	Conv layer	kernel size = 64, stride = 2	
Distilling	Pooling layer	kernel size = 3, stride = 2	$32 \times 496$
	2xMSCAL	B1 size = 5, B2 size = 3, stride = 1	
MSTFF block #1	2xTFFN	$\gamma = 0.1$	$32 \times 496$
	Conv layer	kernel size = 5, stride = 1	
Distilling	Pooling layer	kernel size = 3, stride = 2	$64 \times 247$
	2xMSCAL	B1 size = 5, B2 size = 3, stride = 1	
MSTFF block #2	2xTFFN	$\gamma = 0.1$	$64 \times 247$
	Conv layer	kernel size = 5, stride = 1	
Distilling	Pooling layer	kernel size = 3, stride = 2	$128 \times 123$
	2xMSCAL	B1 size = 5, B2 size = 3, stride = 1	
MSTFF block #3	2xTFFN	$\gamma = 0.1$	$128 \times 123$
	Conv layer	kernel size = 5, stride=1	
Distilling	Pooling layer	kernel size = 3, stride = 2	$256 \times 61$
	2xMSCAL	B1 size = 5, B2 size = 3, stride = 1	
MSTFF block #4	2xTFFN	$\gamma = 0.1$	$256 \times 61$
	Flatten layer	/	15616
Classifier	Linear layer	/	256
	Linear layer	/	$C$

6226R CPU and a GTX 4090 GPU. FE-MCFormer employs the cross-entropy loss function and uses the Adam optimizer to accelerate the training process. The learning rate is set to 0.001, and the batch size is set to 64 in the experiment.

The following max-min normalization operation is applied to mitigate the effects of various magnitude of the measured values on the modeling accuracy:

$$\tilde{x} = \frac{x - x_{min}}{x_{max} - x_{min}} \quad (18)$$

where  $\tilde{x}$  is the normalized value of the measured variable  $x$ ;  $x_{max}$  and  $x_{min}$  are the maximum and minimum values within the array, respectively. Accuracy is used as a metric to evaluate fault diagnosis performance, can be defined as:

$$Acc = \frac{TP}{TP + FP} \times 100\% \quad (19)$$

where  $TP$  and  $FP$  are true positive and false positive of the diagnostic results, respectively. To evaluate the robustness of

**Table 2**  
Description of PU dataset (Case 1)

Category	Bearing	Damage	Level	Method	Label
0	K001	Normal	/	/	$H_1$
1	K002	Normal	/	/	$H_2$
2	K003	Normal	/	/	$H_3$
3	K004	Normal	/	/	$H_4$
4	K005	Normal	/	/	$H_5$
5	K006	Normal	/	/	$H_6$
6	KA01	Outer ring	1	EDM damage	$H_7$
7	KA03	Outer ring	2	electric engraver	$H_8$
8	KA05	Outer ring	1	EDM damage	$H_9$
9	KA06	Outer ring	2	electric engraver	$H_{10}$
10	KA07	Outer ring	1	drilling	$H_{11}$
11	KA08	Outer ring	2	drilling	$H_{12}$
12	KA09	Outer ring	2	drilling	$H_{13}$
13	KI01	Inner ring	1	EDM damage	$H_{14}$
14	KI03	Inner ring	1	electric engraver	$H_{15}$
15	KI05	Inner ring	1	electric engraver	$H_{16}$
16	KI07	Inner ring	2	electric engraver	$H_{17}$
17	KI08	Inner ring	2	electric engraver	$H_{18}$

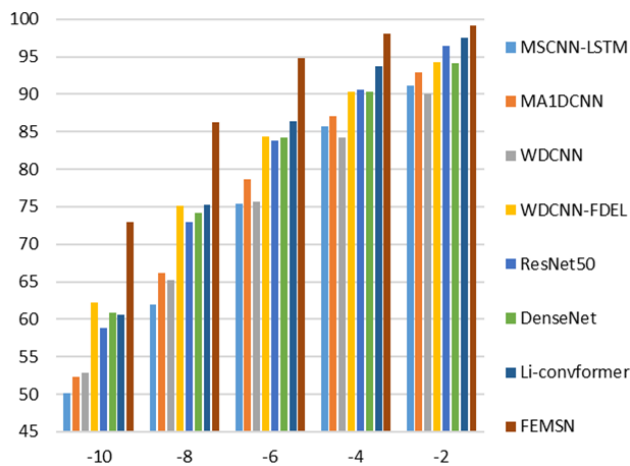


**Fig. 3.** Test results of rolling bearing dataset in Case 1.

FE-MCFormer under noisy environment, different degrees of Gaussian white noise are added to the raw mechanical signals to construct noisy signals with various signal-to-noise ratios (SNR). The SNR is defined as follows:

$$SNR = 10 \lg \left( \frac{P_s}{P_n} \right) \quad (20)$$

$$P_s = \frac{1}{N} \sum_{n=1}^N |v(n)|^2 \quad (21)$$

where  $P_n$  and  $P_s$  denote the power of the raw signal and noisy signal, and  $v(n)$  represents the raw signal. In this experiment, the SNR is set in the range of  $-10$  dB to  $-2$  dB. Each group

of experiments is repeated five times, and the epoch of each experiment is set to 200. Table 1 shows the layer size of each module in MF-MCFormer. In the  $l$ th MSTFF block,  $B_1$  and  $B_2$  size denote the  $1 \times 3$  and  $1 \times 5$  convolution kernel in Eq.(9);  $\gamma = 0.1$  denotes the value of scaling factor  $\gamma$  in Eq. (5) and Eq. (14) is settled to 0.1;  $C$  represents the number of classes in each dataset.

### 3.2. Case 1: Rolling bearing dataset

#### 3.2.1. Dataset description

The bearing dataset [29] collected by Paderborn University (PU) is used in this case to validate the proposed FE-MCFormer method under strong noise and variation working condition. Fig. 2 shows the rolling bearing health monitoring test bench, which mainly consists of an induction motor, a load motor, a measurement shaft and a control panel. The deep groove ball bearing is used as the experimental object. Under a torque load of 0.7 Nm, the induction motor runs at a speed of 1500 rpm with a sampling frequency of 64 kHz in the experiment. The 18 states for the bearing described in Table 2 are employed in this example, including 6 normal states, 7 outer ring failures and 5 inner ring failures. The total of 1000 samples is randomly selected for each state, of which 800 samples are used for model training, while the rest are used for testing. As such, there is a total of  $18 \times 1000 = 18,000$  samples, each containing 2048 vibration points.

#### 3.2.2. Result analysis

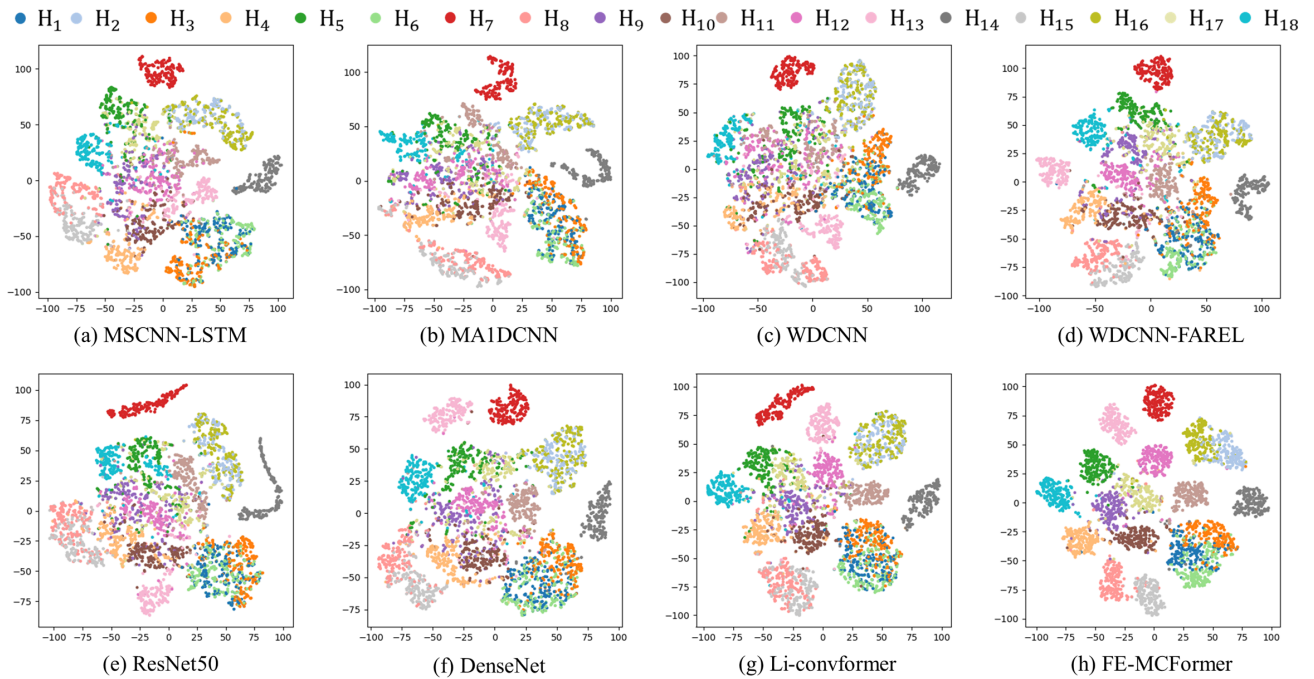
Seven deep learning (DL) approaches, namely MCNN-LSTM [30], MA1DCNN [31], WDCNN, WDCNN-FAREL, ResNet50 [32], Densenet and Li-convformer [33], are employed in the comparison study with FE-MCFormer. As shown in Table 3 and Fig. 3, it can be observed that FE-MCFormer yields the best bearing diagnostic performance under various SNR noise levels, indicating the superiority of the proposed FE-MCFormer over the existing DL methods. More specifically, FE-MCFormer achieves diagnostic accuracy of 99.11%, 98.01%, and 94.74% under SNR levels ranging from  $-2$  dB to  $-6$  dB. The maximum accuracy of FE-MCFormer under SNR values of  $-2$  dB,  $-4$  dB, and  $-6$  dB can reach up to 99.37%, 98.16%, and 94.93%, respectively, which represents a promising result for fault diagnostics (FD). Moreover, FE-MCFormer maintains high accuracy even under extremely noisy environments, further illustrating its strong robustness. Fig. 4 shows the 2D T-SNE visualization results of various methods under SNR =  $-6$  dB, illustrating tight clustering of various faults with high category recognition, confirming FE-MCFormer's feasibility in complex industrial environment.

MSCNN-LSTM and MA1DCNN, as the state-of-the-art multiscale convolutional networks, exhibit outstanding performance under weak noise conditions, reaching 92.22% and 93.86% max accuracy at the SNR of  $-2$  dB, respectively. However, as the noise level increases from  $-2$  dB to  $-6$  dB, their accuracy drops significantly. In contrast, the proposed FE-MCFormer achieves diagnostic accuracy of 99.11%, 98.01%, and 94.74% under the SNR level ranging from  $-2$  dB to  $-6$  dB. Numerical results indicate that, in

**Table 3**

Test results of various deep learning methods on PU dataset in Case 1 (%)

Methods	SNR=-10		SNR=-8		SNR=-6		SNR=-4		SNR=-2	
	mean-acc	max-acc								
MSCNN-LSTM	50.17	52.87	61.90	66.33	75.39	80.38	85.65	87.13	91.13	92.22
MA1DCNN	52.37	52.76	66.11	69.26	78.65	80.61	87.01	89.16	92.89	93.86
WDCNN	52.81	53.97	65.23	66.00	75.70	77.71	84.23	85.14	90.01	90.95
WDCNN-FAREL	62.19	62.69	75.15	75.70	84.41	85.06	90.28	90.54	94.32	94.58
ResNet50	58.85	59.45	72.90	73.80	83.86	84.66	90.57	91.04	96.49	97.03
DensNet	60.81	61.33	74.11	74.87	84.15	84.47	90.31	91.41	94.15	94.71
Li-convformer	60.65	61.02	75.28	75.84	86.34	86.50	93.79	93.88	97.53	97.77
<b>FE-MCFormer</b>	<b>72.99</b>	<b>73.67</b>	<b>86.31</b>	<b>86.80</b>	<b>94.74</b>	<b>94.93</b>	<b>98.01</b>	<b>98.16</b>	<b>99.11</b>	<b>99.37</b>

**Fig. 4.** Results of 2D T-SNE visualization on rolling bearing dataset under SNR = -6 (Case 1).

noisy environments, the multiscale kernels in the multiscale convolutional neural networks (MSCNN) tend to amplify both high frequency noise patterns and key local features, resulting in redundant and conflicting weight distribution. This makes it difficult for the model to focus on critical fault features, leading to degraded performance in FD of rotating machines. In contrast, the proposed FE-MCFormer leverages FAREL and TFFN to suppress irrelevant frequency components, and employs MSAL to strengthen local multiscale feature representations, thereby achieving superior performance over MSCNNs.

The classical WDCNN uses large kernels to construct global dependency, thus reducing the noise interference. However, due to the limitation of the convolution kernel, the model struggles to fully capture long-range dependencies over the entire signal sequence. The WDCNN-FAREL

introduces the proposed FAREL to enhance the global dependency ability, which shows significant improvement compared with the original WDCNN. More specifically, as shown in Table 3, after introducing the FAREL, the mean accuracy of WDCNN under SNR = -2, -4, -6, -8, -10 are 94.32%, 90.28%, 84.41%, 75.15% and 62.19%, respectively, 4.31%, 6.00%, 8.71%, 9.92% and 9.38% higher than those of the baseline WDCNN. Fig. 4 further visually illustrates that the WDCNN-FAREL has higher clustering ability compared with the original WDCNN. Such improvements highlight the effectiveness of FAREL as a general enhancement component for neural network (NN) based fault diagnosis, which adaptively encodes global frequency information through gradient optimization, and improves accuracy without requiring experimental expertise. Meanwhile, when comparing FE-MCFormer with WDCNN-FAREL, FE-MCFormer

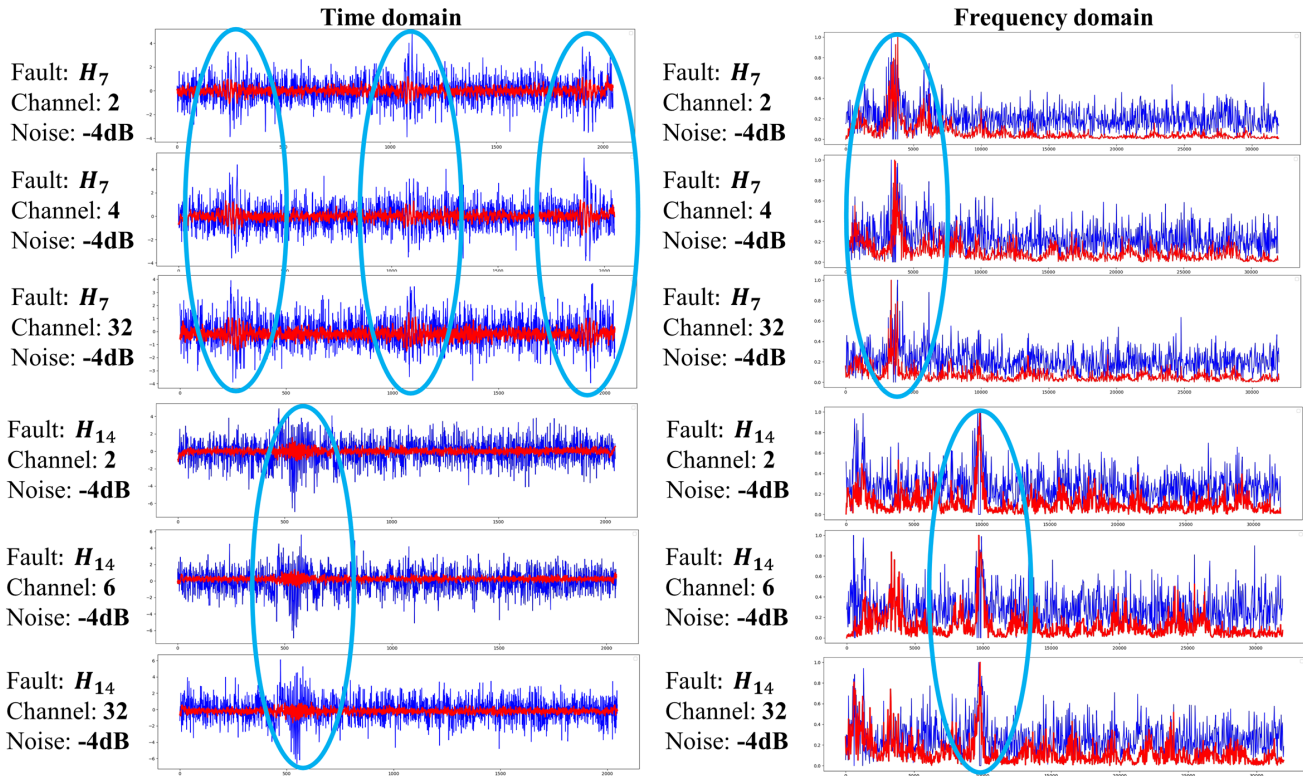


Fig. 5. Reconstruction results of bearing fault signal under SNR = -4 dB (Case 1).

consistently achieves higher accuracy under all noise conditions, indicating the superiority of other components in FE-MCFormer.

Compared with Resnet50 and Densenet, FE-MCFormer has the higher accuracy across all noise scenarios. More specifically, small convolution kernels in Resnet50 and Densenet are easily interfered by the noise signal, because of their limited receptive field. In contrast, the proposed method utilizes advanced network architecture to enhance the model's global dependency and nonlinear ability, thus achieving the higher performance. From Table 3, the average accuracy of FE-MCFormer under SNR = -2, -4, -6, -8, -10 are 99.11%, 98.01%, 94.74%, 86.31% and 72.99%, respectively, higher than ResNet's 96.49%, 90.57%, 83.86%, 72.90% and 58.85%, while 4.96%, 7.70%, 10.59%, 12.20% and 12.18% higher than DenseNet. These results demonstrate the superiority of FE-MCFormer when comparing with classical DL model.

Li-convformer, as the state-of-the-art transformer network, shows outstanding performance under weak noise conditions, achieving 97.77%, 93.88%, and 86.50% accuracy at the SNR of -2, -4, -6 dB, respectively. However, as the noise level increases, the accuracy drops significantly. In contrast, the proposed FE-MCFormer achieves the diagnostic accuracy of 99.11%, 98.01%, and 94.74% under the SNR levels ranging from -2 dB to -6 dB. The maximum accuracy of FE-MCFormer under the SNR values of -2 dB, -4 dB, and -6 dB can reach as high as 99.37%, 98.16%, and 94.93%, respectively, which represents a promising tool for

FD of rotating machines. Moreover, FE-MCFormer maintains a certain level of performance even in extreme noise environments.

In conclusion, compared to other DL models that rely solely on time-domain feature extraction, FE-MCFormer integrates global frequency-domain reconstruction with multi-scale time-domain feature extraction. This combination enables FE-MCFormer to maintain high accuracy, even under strong noise conditions.

To further demonstrate the denoising capability and interpretability of FE-MCFormer, we visually compare the original and reconstructed signals at SNR = -4 dB. Fig. 5 shows reconstruction results for selected channels, where the blue curve denotes the raw noisy signal, while the red curve represents the tensor reconstructed by the FAREL.

The reconstructed signals (red) exhibit substantially smoother profiles with diminished high-frequency components compared to the original signals (blue). This indicates that the proposed FAREL can effectively learn and suppress noise-dominated frequency components while retaining essential features. The normalized frequency-domain plots further confirm that energy levels in the noise bands are greatly attenuated. This indicates that the proposed embedding layer can effectively learn and suppress noise-dominated frequency components while retaining essential features.

**Table 4**  
Ablation result on PU dataset in Case 1

Methods	SNR=-10		SNR=-8		SNR=-6		SNR=-4		SNR=-2	
	mean-acc	max-acc								
FE-MCFormer	72.99	73.67	86.31	86.80	<b>94.74</b>	<b>94.93</b>	<b>98.01</b>	98.16	<b>99.11</b>	<b>99.37</b>
FE-MCFormer-0.2	<b>73.58</b>	<b>74.48</b>	85.45	<b>86.83</b>	94.72	94.71	97.85	<b>98.32</b>	98.93	98.97
FE-MCFormer-0.3	71.42	73.32	<b>86.41</b>	86.72	94.42	94.69	97.84	98.19	99.03	99.15
FE-MCFormer-0.4	73.02	74.26	85.51	86.26	93.79	94.56	97.88	98.06	99.04	99.19
FE-MCFormer-0.5	73.39	74.04	85.54	85.93	94.16	94.41	97.6	97.75	98.67	99.26
FE-MCFormer-0.6	73.03	73.41	85.47	86.67	93.79	94.52	97.44	98.06	98.68	99.10
FE-MCFormer-0.7	72.53	73.65	85.47	86.39	93.26	94.01	97.46	97.95	98.75	98.99
FE-MCFormer-0.8	73.10	73.72	85.53	86.32	92.93	93.84	97.31	97.79	98.8	99.04
Non-MSA	70.78	71.63	82.59	82.90	91.61	92.40	95.81	96.27	98.08	98.27
Non-FFT	69.77	70.57	81.28	81.71	90.99	91.94	95.95	96.59	98.22	98.54
Non-FAREL	70.01	70.97	83.40	84.21	91.83	92.47	96.51	96.84	98.54	99.08

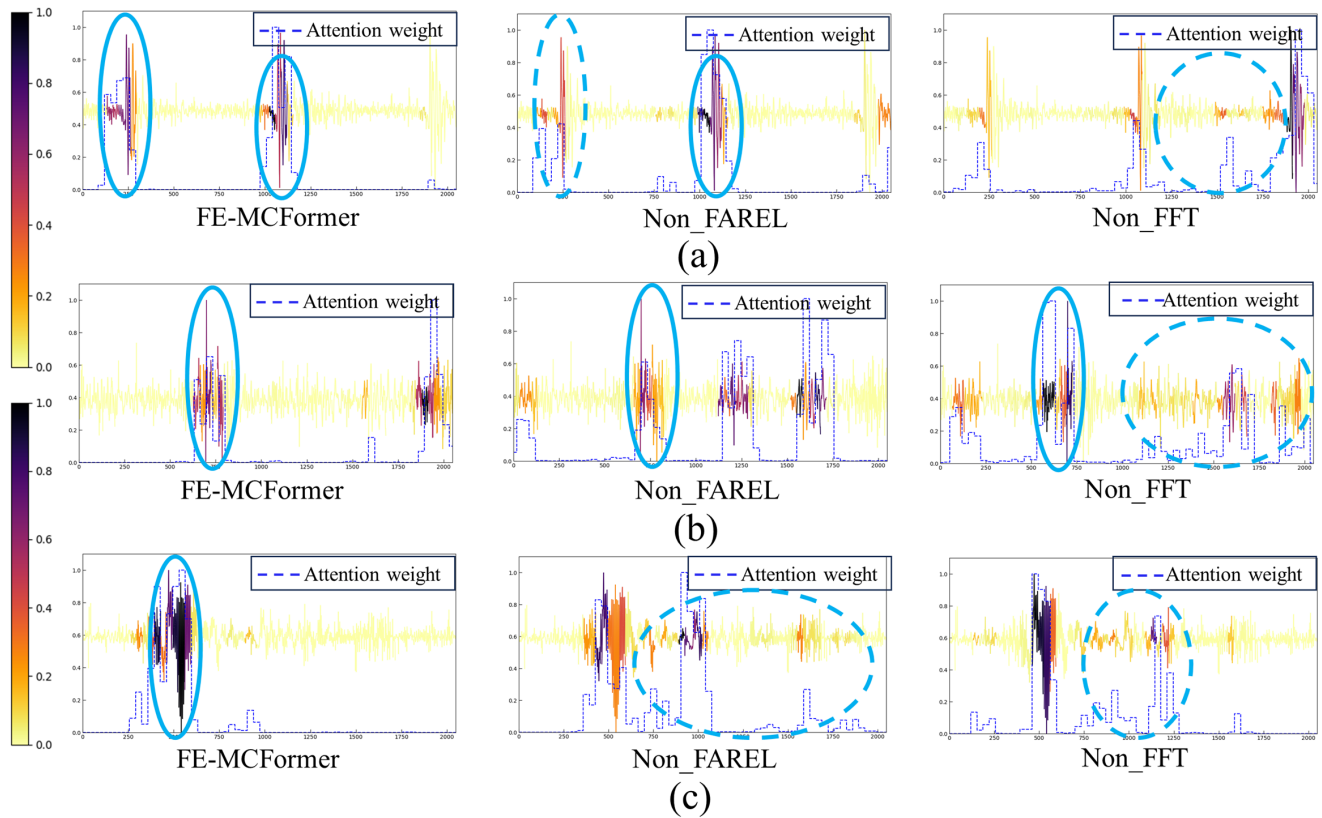


**Fig. 6.** Attention heat map of vibration signals from three states under SNR = -8 dB: (a) KA01, outer ring fault. (b) KA07, outer ring fault. (c) KI01, inner ring fault.

### 3.2.3. Sensitivity analysis and ablation study

To assess the influence of each components in FE-MCFormer, four variant models are established for validation on the PU dataset, named FE-MCFormer- $i$ , Non-MSA, Non-FFT and Non-FAREL. More specifically, in the FE-MCFormer- $i$ , the scaling factor  $\gamma$  in Eq. (5) and Eq. (14) is settled to  $i$ ; Non-MSA denotes that the multiscale attention mechanism of Eq. (8) and Eq. (9) is not used; Non-FFT denotes that the Fourier adaptive reconstruction (FAR)

operations in TFFN are not used; Non-FAREL indicates that the Fourier adaptive reconstruction embedding layer (FAREL) is not used. The ablation results on PU bearing dataset (Case 1) are summarized in Table 4. It can be observed that the addition of scaling factor  $\gamma$ , MSA, FFT and FAREL can effectively improve the accuracy of the model under high noise environments. More specifically, a smaller scaling factor  $\gamma$  leads better model performance. For instance, the original FE-MCFormer with the scaling

factor  $\gamma$  of 0.1 has the highest mean accuracy at SNR =  $-2$ ,  $-4$  and  $-6$  dB, up to 99.11%, 98.01% and 94.74%, respectively; The FE-MCFormer-0.2 and FE-MCFormer-0.3 show the best performance at SNR =  $-10$  and  $-8$ . These results demonstrate that the smaller scaling factors  $\gamma$  achieve the better performance across all noise levels, while the larger scaling factors lead to the worse performance. This demonstrates the importance of introducing scaling factors in both FAREL and TFFN, as they help maintain numerical stability during signal reconstruction.

The introduction of MSA enables the model to fully extract the key multiscale time-domain features from the input features, as shown in Table 4. Compared to the model without MSA mechanism, the FE-MCFormer achieves performance improvements of 2.21%, 3.72%, 3.13%, 2.2% and 1.03% at the SNR levels of  $-10$ ,  $-8$ ,  $-6$ ,  $-4$  and  $-2$  dB, respectively. In MSA, the  $1 \times 3$  and  $1 \times 5$  convolution kernels are introduced to extract local key features and trend patterns. The Hadamard product is utilized to evoke the multiscale attention. Finally, the softmax function is applied to enhance the sparsity and interpretability of the attention maps.

Meanwhile, the FAR and FAREL effectively suppress irrelevant information and establish global dependencies in frequency-domain, which not only improve the diagnosis accuracy of FE-MCFormer, but also enhance the interpretability of MSA under strong noise environment. More specifically, small-kernel convolutions (e.g.,  $1 \times 3$  and  $1 \times 5$ ), which are widely used in NN-based signal processing for rotating machinery, exhibit strong sensitivity to local signal components. This feature enables the small-kernel convolutions to effectively capture impulsive segments caused by rotating machinery faults. As a result, they perform well in fault diagnosis under laboratory conditions with less noise. However, as the noise increases, key local information within the signal becomes obscured, making it difficult for small-kernel convolutions to effectively extract fault features from complex signals, thus leading to a decline in performance, taking FE-MCFormer as an example, when the model excludes FAR or FAREL, the attention matrices within the MSA become easily disturbed by noise, leading to weight dispersion and subsequent performance degradation. To further illustrate this, we visualize the attention heatmaps of first MSA in Eq. (9) in the fourth MSTFF block. The three typical fault states of the attention heatmap under SNR =  $-10$  dB are shown in Fig. 6, the darker color indicates the areas of the signal that the model focuses more.

It can be observed from Fig. 6, under noisy conditions, the attention weight distribution of MSA becomes dilute and unstable. The FE-MCFormer without FAREL or FFT exhibits dispersed attention peaks that frequently respond to background noise rather than fault-related impulses, which is particularly evident in Fig. 6 (b) and (c). This suggests that under strong noise, the attention weights of MSA lose focus on key signal parts, leading to the degradation of both model performance and interpretability. In contrast, FE-MCFormer, which incorporates the TFFN and the FAREL,

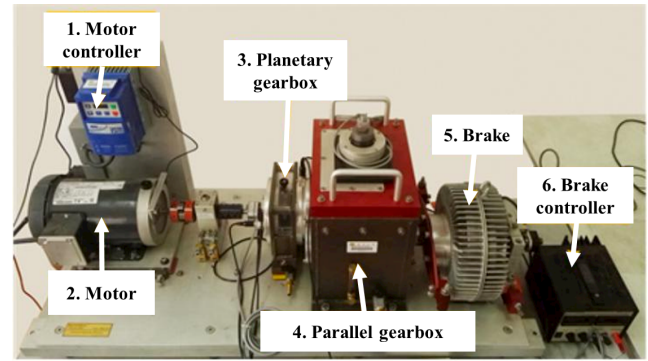


Fig. 7. Gearbox fault test rig. (Case2)

Table 5  
Description of SEU dataset (Case 2)

Category	Location	Type	Description	Label
0	Gearbox	Chipped	Crack occurs in the gear feet	$F_1$
1	Gearbox	Miss	Missing one of feet in the gear	$F_2$
2	Gearbox	Root	Crack occurs in the root of gear feet	$F_3$
3	Gearbox	Surface	Wear occurs in the surface of gear	$F_4$
4	Gearbox	Normal	No fault	$F_5$

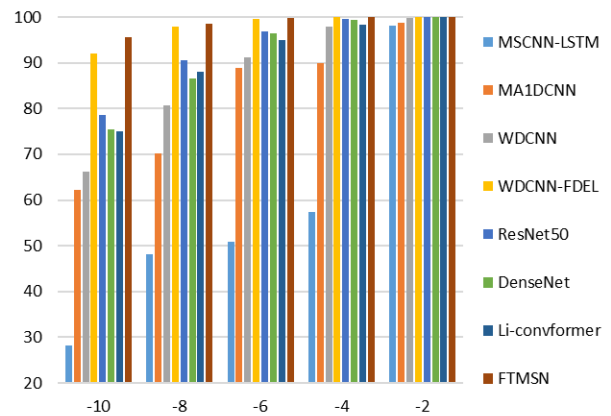


Fig. 8. Test results on SEU dataset (Case 2).

shows highly concentrated attention on the fault impulse regions. This suggests that the introduction of TFFN and FAREL not only enhance the global dependency of FE-MCFormer, but also enhance the model interpretability under strong noise conditions.

### 3.3. Case 2: Gearbox dataset

#### 3.3.1. Dataset description

The Southeast University gearbox dataset (SEU) [34] is employed in this case study to demonstrate the effectiveness of the proposed FE-MCFormer method. The test bench for gearbox health monitoring is shown in Fig. 7. The gearbox data contains 5 fault types in two operating conditions (20 Hz-0 V and 30 Hz-2 V). The detailed description is summarized in Table 5. The total number of samples in this dataset is 5000, of which 4000 samples are selected for model training, and the rest is used for model testing.

**Table 6**  
Test results of various deep learning methods on SEU dataset in Case 2 (%)

Methods	SNR=-10		SNR=-8		SNR=-6		SNR=-4		SNR=-2	
	mean-acc	max-acc	mean-acc	max-acc	mean-acc	max-acc	mean-acc	max-acc	mean-acc	max-acc
MSCNN-LSTM	28.16	42.47	48.18	50.63	50.78	60.74	57.40	92.42	98.10	99.13
MA1DCNN	62.29	64.53	70.22	74.34	88.94	91.35	89.94	98.54	98.81	99.03
WDCNN	66.16	67.15	80.77	81.63	91.11	91.64	97.96	97.48	99.71	99.38
WDCNN-FAREL	91.96	93.20	97.86	98.83	99.61	99.81	100	100	100	100
ResNet50	78.54	79.79	90.61	91.16	96.75	96.89	99.49	99.51	100	100
DenseNet	74.07	75.51	87.97	89.21	96.19	96.50	99.15	99.42	100	100
Li-convformer	75.02	76.68	88.05	88.82	94.97	95.72	98.36	98.51	100	100
<b>FE-MCFormer</b>	<b>95.51</b>	<b>96.31</b>	<b>98.52</b>	<b>98.83</b>	<b>99.79</b>	<b>99.90</b>	<b>100</b>	<b>100</b>	<b>100</b>	<b>100</b>

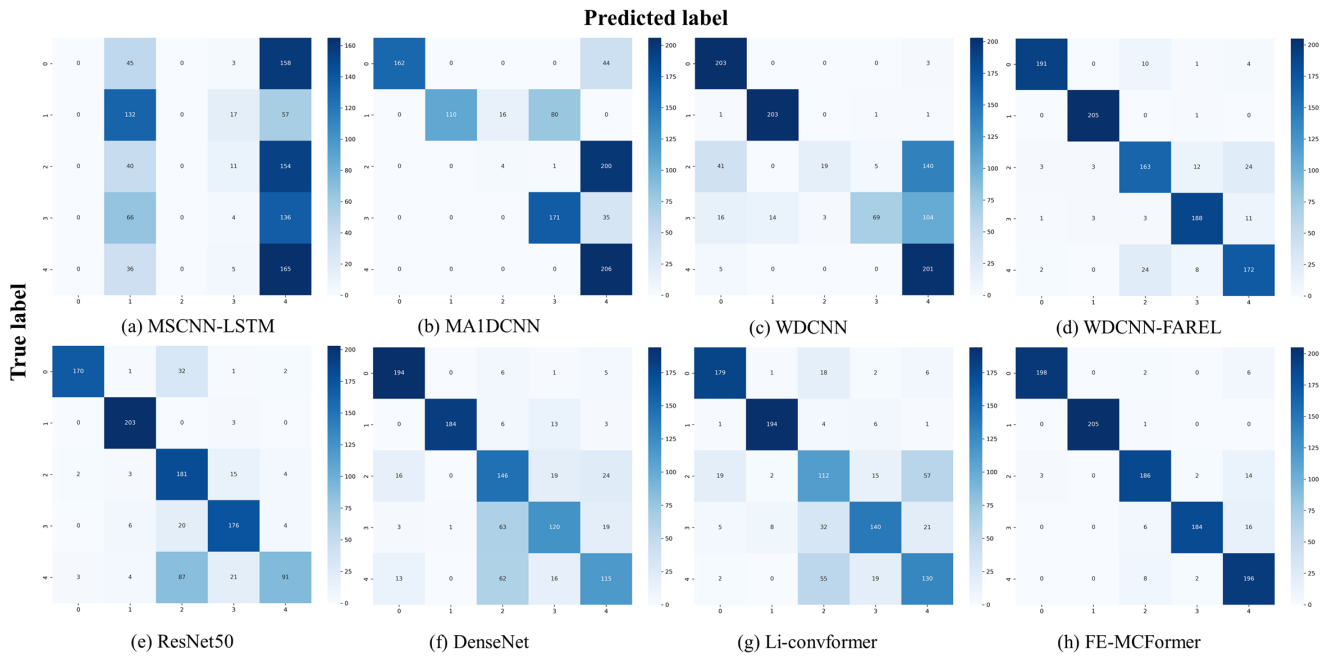


**Fig. 9.** Confusion matrix of gearbox dataset under SNR = -10 dB (Case 2).

### 3.3.2. Result analysis

The experimental results of the SEU dataset are shown in Table 6 and Fig. 8. As shown in Table 6, it can be observed that FE-MCFormer achieves diagnosis accuracies of 100%, 100%, 94.93%, 98.83%, and 95.51% in five trials, each demonstrating the highest accuracy. Even in extreme noisy environments, where SNR = -10 dB, the proposed FE-MCFormer demonstrates an overall improvement of 67.35%, 33.22%, 29.35%, 3.55%, 16.97%, 20.8% and 12.34% compared to MSCNN-LSTM, MA1DCNN, WDCNN, WDCNN-FAREL, ResNet50, Densenet and Li-convformer, respectively. This further demonstrates the strong robustness of the proposed FE-MCFormer. Fig. 9 presents the confusion matrices for FE-MCFormer and CMSN under the noise condition of SNR = -10 dB, where the “Predicted label” represents the predicted result, and the “Ture label” represents the actual class. The darker the bar for the same class, the more accurate the prediction,

and the better the classification performance. As shown in Fig. 9, compared with other state-of-the-art methods, FE-MCFormer demonstrates superior performance in distinguishing various fault types. Meanwhile, it can be observed from Table 6 and Fig. 8 that, the introduction of FAREL significantly improves the overall performance of WDCNN, the WDCNN-FAREL achieves the mean accuracies of 91.96%, 97.86% and 99.61% at the SNR of -10, -8 and -6 dB, respectively, which are 25.8%, 17.09% and 8.5% higher than the baseline WDCNN. Fig. 9 (c) and Fig. 9 (d) demonstrate that the WDCNN-FAREL predicts the categories more correctly than the original WDCNN, further illustrating the effectiveness and generality of FAREL.

The denoising performance of signals across different channels in FE-MCFormer has been presented in Case 1. In this case, the summation and average FAREL output tensors are computed to further demonstrate the overall denoising

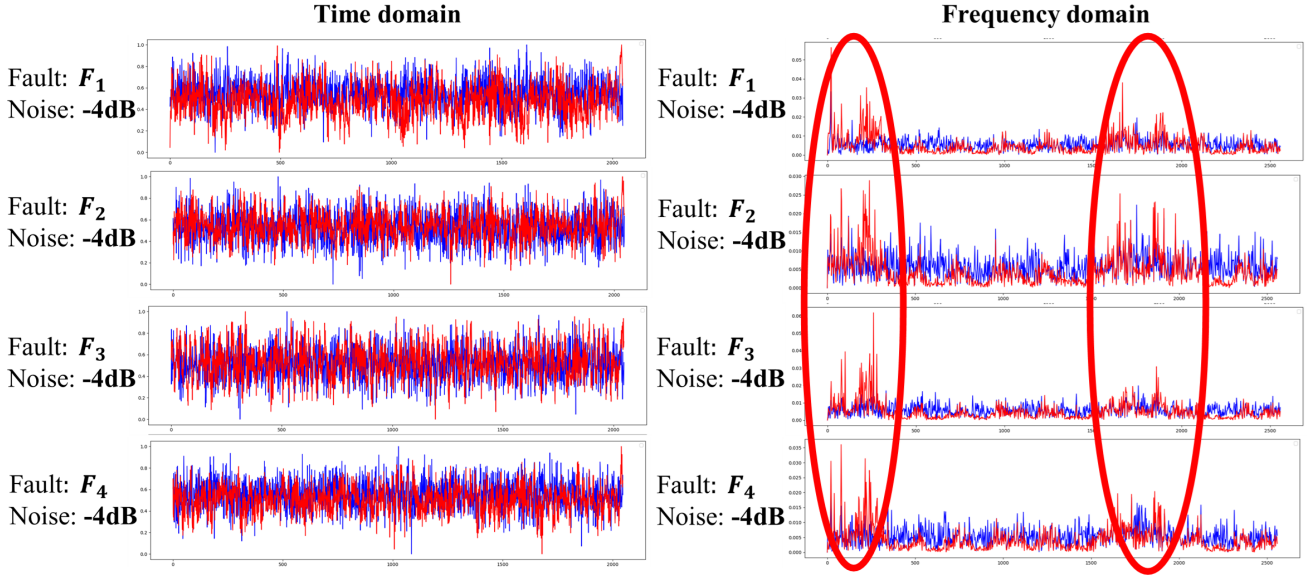


Fig. 10. Reconstruction results of gear fault signals (Case 2).

Table 7

Quality estimation of features for various DL method (Case 2).

Methods	SNR=-10		SNR=-8		SNR=-6		SNR=-4		SNR=-2	
	$J_1$	$J_2$	$J_1$	$J_2$	$J_1$	$J_2$	$J_1$	$J_2$	$J_1$	$J_2$
MSCNN-LSTM	0.73	2.37	1.65	1.6	2.54	1.4	2.48	1.4	6.00	1.17
MA1DCNN	1.21	1.28	2.08	1.47	2.80	1.35	2.76	1.36	2.61	1.38
WDCNN	1.34	1.74	2.02	1.49	2.48	1.40	3.18	1.31	3.47	1.28
WDCNN-FDEL	2.23	1.45	2.64	1.38	3.63	1.27	4.84	1.21	5.15	1.19
ResNet50	1.38	2.38	1.89	2.88	2.23	3.23	2.81	3.82	3.10	4.02
Densenet	1.41	1.70	1.97	1.51	2.41	1.42	2.80	1.36	3.23	1.31
Li-convformer	1.66	1.56	2.20	1.46	2.91	1.34	3.21	1.31	3.32	1.41
FTMSN	<b>3.71</b>	<b>1.27</b>	<b>4.67</b>	<b>1.21</b>	<b>6.21</b>	<b>1.16</b>	<b>9.06</b>	<b>1.11</b>	<b>13.94</b>	<b>1.07</b>

capability. Additionally, BOTH the noisy signals and reconstructed tensors are normalized according to Eq. (18), as shown in Fig. 10. These results demonstrate that the globally reconstructed signal enhances the essential characteristics of the original signal while significantly attenuating the noise, which validates the effectiveness of the global encoding mechanism in enhancing signal interpretability under strong noise conditions.

### 3.3.3. Output quality evaluation

To further demonstrate the superior performance of FE-MCFormer, we evaluate the quality of the output characteristics of various DL methods on the SEU dataset using between-class covariance  $S_b$  and within-class covariance  $S_w$  [33], in which  $S_b$  is defined to evaluate the degree of separation of the different classes,  $S_w$  is utilized to indicate the degree of clustering of the same class. The larger  $S_b$  and the smaller  $S_w$  represent the better feature extraction quality.

$$S_b = \sum_{k=1}^K N_k (\bar{v}_k - \bar{v}_m)(\bar{v}_k - \bar{v}_m)^T \quad (22)$$

$$S_w = \sum_{k=1}^K \sum_{x \in C_k} (x - \bar{v}_k)(x - \bar{v}_k)^T \quad (23)$$

$$\bar{v}_k = \frac{1}{N_k} \sum_{x \in C_k} x \quad (24)$$

$$\bar{v}_m = \frac{1}{N} \sum_{n=1}^N x_n \quad (25)$$

where  $x$  denotes the input tensor,  $k$  represents the total numbers of all health statuses,  $N_k$  represents the size of

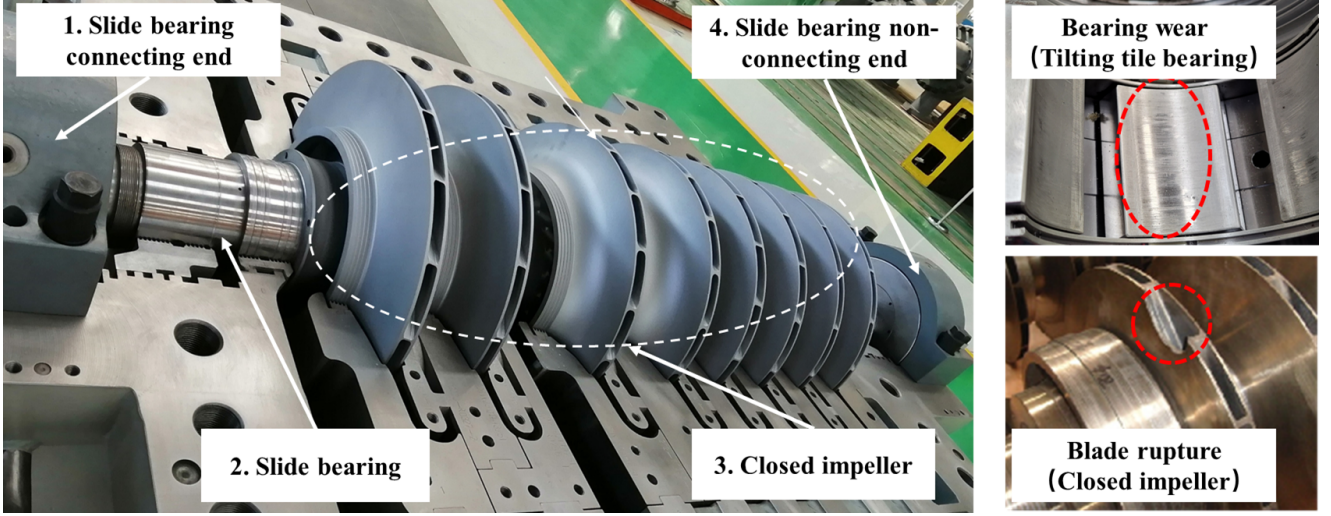


Fig. 11. Illustration of the centrifugal compressor for methodology implementation (Case 3).

**Table 8**  
Description of compressor dataset (Case 3)

Category	Fault	Label	Samples
0	Normal	$C_1$	240
1	Blade rupture	$C_2$	240
2	Bearing wear	$C_3$	240
3	Rotor misalignment	$C_4$	240
4	Oil misalignment	$C_5$	240

samples of class  $C_k$ ,  $v_k$  stands for the average of the feature vector of the class  $C_k$ , and  $v_m$  stands for the average of all samples. Thus, the evaluation metrics  $J_1$  and  $J_2$  can be calculated as

$$J_1 = \frac{S_b}{S_w} \quad (26)$$

$$J_2 = \frac{S_w + S_b}{S_w} \quad (27)$$

Note that the larger the value of the  $J_1$  and the smaller of the value of the  $J_2$ , the better the diagnostic performance.  $J_1$  and  $J_2$  value of FE-MCFormer and other networks are shown in Table 7. At the same SNR levels, FE-MCFormer achieves larger  $J_1$  and smaller  $J_2$  compared with other DL models, confirming its ability to extract fault features with high quality, demonstrating consistent high-performance and robust on fault diagnosis of rotating machines.

### 3.4. Case 3: Centrifugal compressor dataset

#### 3.4.1. Dataset description

This case is employed to demonstrate the feasibility of the proposed FE-MCFormer method for fault diagnosis of large rotating machines with small dataset. Centrifugal compressors, as representative large-scale rotating machinery,

pose great difficulties in fault signal acquisition, leading to insufficient samples for fault diagnosis. In this case, a dataset collected from a real world centrifugal compressor are utilized to verify the feasibility and applicability of the proposed method. The 7200 and 3300 eddy current probes are utilized to acquire the bearing displacement signals; the sampling frequency is set to 30000 Hz. In this study, the axial displacement data along the x-direction of the compressor bearing are collected under five operating conditions, including four fault states and one normal state, each having 240 samples, as summarized in Table 8. Representative fault modes of the centrifugal compressor unit are illustrated in Fig. 11, such as bearing wear and blade rupture. 192 samples from each state are randomly selected for model training, and the rest are used for model testing. All signals are normalized according to Eq. (18).

#### 3.4.2. Results analysis

In this case, no additional noise is added to the raw signal for model evaluation because the data are collected from actual operating conditions. Table 9 reports the diagnostic performance of various methods in this case. It is observed from Table 9 that the proposed model maintains the best accuracy and output quality even under complex noisy conditions with a small number of samples. This is mainly attributed to the specific design of the FE-MCFormer structure. By incorporating lightweight MSCAL and TFFN modules, FE-MCFormer significantly reduces the risk of overfitting under small-sample conditions. Meanwhile, its strong noise robustness allows the model to effectively process noisy signals from large-scale rotating machinery operating under high-speed and heavy-load conditions.

#### 3.4.3. Interpretable analysis

To further validate the interpretability and effectiveness of the proposed FE-MCFormer in real industrial environments, we compare the frequency spectra of the original and reconstructed signals of FAREL, as shown in Fig. 12,

**Table 9**  
Test results on the compressor dataset (Case 3)

Score	MSCNN-LSTM	MA1DCNN	WDCNN	WDCNN-FAREL	ResNet50	Densenet	Li-convformer	FE-MCFormer
Mean-acc (%)	79.38	80.74	89.63	94.89	89.58	96.48	95.43	<b>96.89</b>
Max-acc (%)	80.17	87.04	91.2	95.83	90.28	97.22	95.83	<b>97.37</b>
$J_1$	0.35	2.28	2.78	3.09	2.20	1.36	2.85	<b>3.11</b>
$J_2$	3.83	1.44	1.36	1.31	1.45	1.73	1.35	<b>1.32</b>

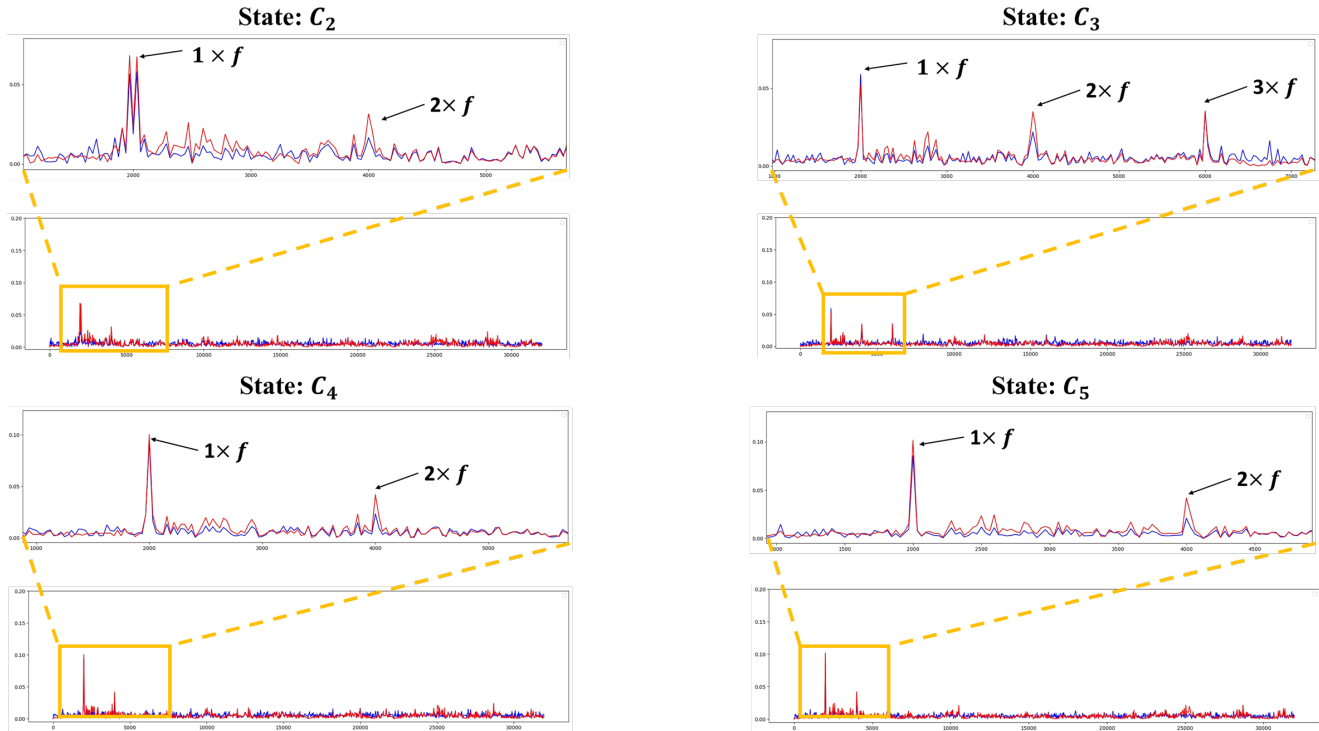


**Fig. 12.** Reconstruction results of the compressor dataset (Case 3).

where the blue curves represent the original spectra, while the red ones correspond to the reconstructed signals. It can be clearly observed from Fig. 12 that the reconstructed signals exhibit significantly enhanced energy at key harmonic positions, such as  $1 \times f$ ,  $2 \times f$  and  $3 \times f$ . This indicates that the model is capable of accurately identifying and retaining periodic frequency components that are strongly correlated with the mechanical state. The consistent enhancement across multiple fault types demonstrates the model's ability to perceive physically meaningful diagnostic patterns.

#### 4. Concluding remarks

The fault diagnostics (FD) of rotating machinery become particularly challenging when considering the influence of strong noise. Most deep learning (DL) methods fail to fully explore the time-frequency features of input signals, resulting in poor performance under noisy conditions. To address

this issue, this study proposes a frequency-enhanced multi-scale transformer (FE-MCFormer) model for FD of rotating machinery under strong noise environments.

First, a Fourier adaptive reconstruction embedding layer (FAREL) is introduced to fully explore global frequency features while filtering out irrelevant information. Next, a multiscale time-frequency fusion (MSTFF) module is employed to extract multiscale time-domain information and global frequency-domain features. Additionally, a distillation layer is incorporated to expand the receptive field. Considering these factors, an end-to-end deep learning model named FE-MCFormer is developed based on the proposed improvements.

The efficacy and interpretability of FE-MCFormer are validated through case studies using three different datasets. Compared with seven other DL methods, FE-MCFormer achieves superior diagnostic results and demonstrates strong noise robustness. For example, on the bearing dataset and gearbox dataset, the FE-MCFormer achieves the highest accuracy of 94.74% and 99.79%, respectively. Meanwhile, on the compressor dataset with a limited number of samples,

FE-MCFormer achieves 96.89% mean accuracy, higher than other DL methods, illustrate its strong potential for deployment in real-world industrial condition monitoring. Furthermore, comparative experiments are conducted to demonstrate the necessity of each component in FE-MCFormer and the generalization ability of FAREL on other DL methods. Interpretability analysis in both the time and frequency domains further reveal the internal mechanisms of the proposed FE-MCFormer.

In future work, we will focus on expanding the application field and further enhancing the interpretability and noise robustness of both FAREL and FE-MCFormer.

## Acknowledgements

This work was supported in part by the Shenyang and Dalian Department of Science and Technology under Grant (No. ZX20221153, 2022RG10), in part by the Provincial Key Lab of Digital Twin for Industrial Equipment under Grant No. 85129003 and in part by the autonomous research project of State Key Laboratory of Structural Analysis, Optimization and CAE Software for Industrial Equipment under Grant No. 202000.

## References

- [1] Lei, Y., Yang, B., Jiang, X., Jia, F., Li, N., Nandi, A.K., 2020. Applications of machine learning to machine fault diagnosis: A review and roadmap. *Mech. Syst. Signal Process.* 138, 106587.
- [2] Ahmad, H., Cheng, W., Wang, W., Zhang, S., Nie, Z., Liu, H., Chen, X., 2025. Consistency-regularized-label-aware contrastive learning with uncertainty-aware periodic pseudo-labeling for machinery fault diagnosis under limited labeled data. *Adv. Eng. Inform.* 68, 103656.
- [3] Zhao, L., Qi, J., Wu, F., Wang, Y., Qin, Y., 2026. Physics modeling-driven interpretable data augmentation method for bearing fault diagnosis under imbalanced data. *Adv. Eng. Inform.* 70, 104189. URL: <https://www.sciencedirect.com/science/article/pii/S1474034625010821>, doi:<https://doi.org/10.1016/j.aei.2025.104189>.
- [4] Jiang, Z., Zhang, K., Xiang, L., Yu, G., Xu, Y., 2023. A time-frequency spectral amplitude modulation method and its applications in rolling bearing fault diagnosis. *Mech. Syst. Signal Process.* 185, 109832. doi:[10.1016/j.ymssp.2022.109832](https://doi.org/10.1016/j.ymssp.2022.109832).
- [5] Xu, Y., Hu, J., 2019. Weak fault detection of rolling bearing using a ds-based adaptive spectrum reconstruction method. *J. Instrum.* 14, P03022.
- [6] Chen, Z., Yang, Y., He, C., Liu, Y., Liu, X., Cao, Z., 2023. Feature extraction based on hierarchical improved envelope spectrum entropy for rolling bearing fault diagnosis. *IEEE Trans. Instrum. Meas.* 72, 1–12. doi:[10.1109/TIM.2023.3277938](https://doi.org/10.1109/TIM.2023.3277938).
- [7] Kou, Z., Yang, F., Wu, J., Li, T., 2020. Application of ICEEMDAN energy entropy and AFSA-SVM for fault diagnosis of hoist sheave bearing. *Entropy* 22, 1347. doi:[10.3390/e22121347](https://doi.org/10.3390/e22121347).
- [8] Zhou, J., Chen, C., Guo, J., Wang, L., Liu, Z., Feng, C., 2023. A novel rolling bearing fault diagnosis method based on continuous hierarchical fractional range entropy. *Measurement* 220, 113395. doi:[10.1016/j.measurement.2023.113395](https://doi.org/10.1016/j.measurement.2023.113395).
- [9] Ren, C., Jiang, B., Lu, N., Simani, S., Gao, F., 2024. Meta-learning with distributional similarity preference for few-shot fault diagnosis under varying working conditions. *IEEE Trans. Cybern.* 54, 2746–2756. doi:[10.1109/TCYB.2023.3338768](https://doi.org/10.1109/TCYB.2023.3338768).
- [10] Chen, J., Hu, W., Cao, D., Zhang, Z., Chen, Z., Blaabjerg, F., 2023. A meta-learning method for electric machine bearing fault diagnosis under varying working conditions with limited data. *IEEE Trans. Ind. Inf.* 19, 2552–2564. doi:[10.1109/TII.2022.3165027](https://doi.org/10.1109/TII.2022.3165027).
- [11] Zhang, L., Wang, B., Liang, P., Yuan, X., Li, N., 2023. Semi-supervised fault diagnosis of gearbox based on feature pre-extraction mechanism and improved generative adversarial networks under limited labeled samples and noise environment. *Adv. Eng. Inform.* 58, 102211. doi:[10.1016/j.aei.2023.102211](https://doi.org/10.1016/j.aei.2023.102211).
- [12] He, C., Gai, N., Yan, K., Shao, H., 2026. A hybrid cross-domain few-shot bearing fault diagnosis method combining multi-scale feature association and physical information. *Adv. Eng. Inform.* 69, 104077.
- [13] Wang, H., Zhou, Z., Zhang, L., Yan, R., 2024. Multiscale deep attention q network: A new deep reinforcement learning method for imbalanced fault diagnosis in gearboxes. *IEEE Trans. Instrum. Meas.* 73, 1–12. doi:[10.1109/TIM.2023.3338664](https://doi.org/10.1109/TIM.2023.3338664).
- [14] Xu, Y., Yan, X., Feng, K., Sheng, X., Sun, B., Liu, Z., 2022. Attention-based multiscale denoising residual convolutional neural networks for fault diagnosis of rotating machinery. *Reliab. Eng. Syst. Saf.* 226, 108714. doi:[10.1016/j.ress.2022.108714](https://doi.org/10.1016/j.ress.2022.108714).
- [15] Jia, L., Chow, T.W.S., Wang, Y., Yuan, Y., 2022. Multiscale residual attention convolutional neural network for bearing fault diagnosis. *IEEE Trans. Instrum. Meas.* 71, 1–13. doi:[10.1109/TIM.2022.3196742](https://doi.org/10.1109/TIM.2022.3196742).
- [16] Yuan, Y., Han, Y., Xiao, K., Xu, Z., Jiang, X., 2025. Remaining useful life prediction for the harmonic reducer of industrial robots via in-situ current signal and lightweight multiscale attention deep networks. *Journal of Manufacturing Systems* 83, 322–336. URL: <https://www.sciencedirect.com/science/article/pii/S0278612525002353>, doi:<https://doi.org/10.1016/j.jmsy.2025.09.008>.
- [17] Li, Y., Zhou, Z., Sun, C., Chen, X., Yan, R., 2024. Variational Attention-Based Interpretable Transformer Network for Rotary Machine Fault Diagnosis. *IEEE Trans. Neural Netw. Learning Syst.* 35, 6180–6193.
- [18] Ding, Y., Jia, M., Miao, Q., Cao, Y., 2022. A novel time–frequency Transformer based on self–attention mechanism and its application in fault diagnosis of rolling bearings. *Mechanical Systems and Signal Processing* 168. Publisher: Elsevier BV.
- [19] Zhang, Y., Zhao, X., Peng, Z., Xu, R., Chen, P., 2025. Wd-kantf: An interpretable intelligent fault diagnosis framework for rotating machinery under noise environments and small sample conditions. *Adv. Eng. Inform.* 66, 103452.
- [20] Han, S., Shao, H., Cheng, J., Yang, X., Cai, B., 2023. Convformer-NSE: A novel end-to-end gearbox fault diagnosis framework under heavy noise using joint global and local information. *IEEE/ASME Trans. Mechatron.* 28, 340–349. doi:[10.1109/TMECH.2022.3199985](https://doi.org/10.1109/TMECH.2022.3199985).
- [21] Khanam, R., Hussain, M., 2024. YOLOv11: An overview of the key architectural enhancements. URL: <http://arxiv.org/abs/2410.17725>, arXiv:2410.17725 [cs].
- [22] Szegedy, C., Ioffe, S., Vanhoucke, V., Alemi, A., 2017. Inception-v4, inception-resnet and the impact of residual connections on learning. *AAAI* 31.
- [23] Zhou, T., Yao, D., Yang, J., Meng, C., Li, A., Li, X., 2024. DRSwint-ST: An intelligent fault diagnosis framework based on dynamic threshold noise reduction and sparse transformer with shifted windows 250, 110327.
- [24] Beltagy, I., Peters, M.E., Cohan, A., 2020. Longformer: The long-document transformer.
- [25] Dong, Y., Cordonnier, J.B., Loukas, A., 2023. Attention is not all you need: Pure attention loses rank doubly exponentially with depth. URL: <http://arxiv.org/abs/2103.03404>, doi:[10.48550/arXiv.2103.03404](https://doi.org/10.48550/arXiv.2103.03404), arXiv:2103.03404 [cs].
- [26] Pires, T., Vilarinho Lopes, A., Assogba, Y., Setiawan, H., 2023. One wide feedforward is all you need, in: *Proceedings of the Eighth Conference on Machine Translation, Association for Computational Linguistics*. pp. 1031–1044.
- [27] Lee-Thorp, J., Ainslie, J., Eckstein, I., Ontanon, S., 2022. FNet: Mixing tokens with fourier transforms. URL: <http://arxiv.org/abs/2105.03824>, doi:[10.48550/arXiv.2105.03824](https://doi.org/10.48550/arXiv.2105.03824), arXiv:2105.03824 [cs].
- [28] Zhai, S., Talbott, W., Srivastava, N., Huang, C., Goh, H., Zhang, R., Susskind, J., 2021. An attention free transformer. URL: <http://arxiv.org/abs/2105.14103>, doi:[10.48550/arXiv.2105.14103](https://doi.org/10.48550/arXiv.2105.14103), arXiv:2105.14103 [cs].

- [29] Lessmeier, C., Kimotho, J.K., Zimmer, D., Sextro, W., 2016. Condition monitoring of bearing damage in electromechanical drive systems by using motor current signals of electric motors: A benchmark data set for data-driven classification, in: PHM society European conference.
- [30] Chen, X., Zhang, B., Gao, D., 2021. Bearing fault diagnosis base on multi-scale cnn and lstm model. *J. Intell. Manuf.* 32, 971–987.
- [31] Wang, H., Liu, Z., Peng, D., Qin, Y., 2020. Understanding and learning discriminant features based on multiattention 1dcnn for wheelset bearing fault diagnosis. *IEEE Trans. Ind. Inf.* 16, 5735–5745. doi:10.1109/TII.2019.2955540.
- [32] Zhao, Z., Li, T., Wu, J., Sun, C., Wang, S., Yan, R., Chen, X., 2020. Deep learning algorithms for rotating machinery intelligent diagnosis: An open source benchmark study. *ISA Trans.*
- [33] Yan, S., Shao, H., Wang, J., Zheng, X., Liu, B., 2024. LiConvFormer: A lightweight fault diagnosis framework using separable multiscale convolution and broadcast self-attention. *Expert Systems with Applications* 237, 121338. doi:10.1016/j.eswa.2023.121338.
- [34] Shao, S., McAleer, S., Yan, R., Baldi, P., 2018. Highly accurate machine fault diagnosis using deep transfer learning. *IEEE Trans. Ind. Inf.* 15, 2446–2455.